

Kinetic energy of ions after Coulomb explosion of clusters induced by an intense laser pulse

Md. Ranaul Islam, Ulf Saalmann, and Jan M. Rost

Max Planck Institute for the Physics of Complex Systems, Nöthnitzer Straße 38, 01187 Dresden, Germany

(Received 22 September 2005; published 17 April 2006)

It is shown that the kinetic-energy distribution of ions emerging from a cluster target irradiated by an intense laser pulse arises from three main effects: (1) the spatial profile of the laser beam, (2) the cluster size distribution in the experiment, and (3) possible saturation effects in the cluster ionization. Our model reveals that each of these effects leaves a characteristic fingerprint in the ion kinetic-energy spectrum. Moreover, it provides a quantitative link between observable ion spectra under experimental conditions and the ideal single-cluster result of a typical calculation.

DOI: [10.1103/PhysRevA.73.041201](https://doi.org/10.1103/PhysRevA.73.041201)

PACS number(s): 36.40.Sx, 33.80.Wz, 36.40.Wa, 52.38.Kd

The interaction of strong femtosecond laser pulses with atomic clusters has been of topical interest for many years [1,2]. Initiated by exciting experimental observations, the understanding of the involved many-particle dynamics remains challenging and has prompted various theoretical approaches ranging from phenomenological models [3,4] to large-scale microscopic calculations [5–7]. Progress in comparison to experiment, and consequently in our understanding of the underlying cluster dynamics, is seriously hampered by the fact that the idealized (but almost always considered) theoretical scenario of a single, well-characterized cluster irradiated by a laser pulse of a given intensity is usually far from the real experimental situation. There, clusters of different size exposed to different intensities contribute to what is finally measured. Theoretical approaches should account for this integral character of the measurements. In extreme cases it is just this convolution that produces the observed features.

A basic and important observable, measured in a number of experiments on atomic and molecular clusters exposed to strong laser pulses [8–14], is the kinetic-energy distributions of ions (KEDI). The fragment ions result from the complete disintegration of the cluster. Despite the fact that atomic species, cluster size, and laser pulse parameters were different in these measurements, the KEDI share similarities such as the increase towards small energies and a tail for large energies. In the following we will derive analytically the characteristic shape of the measured KEDI and discuss how details of these spectra provide insight into the ionization dynamics of the clusters involved. We will show that the spatial profile of the laser beam, the cluster size distribution in the experiment, as recently discussed for proton emission in the Coulomb explosion of hydrogen clusters [13] and nuclear fusion from explosions of deuterium clusters [15], and possible saturation effects in the ionization influence the measured KEDI in a characteristic manner. This is illustrated schematically by an overview in Fig. 1, using scaled energies (see below for their definitions). The panel in Fig. 1(a) shows an “ideal” KEDI from a single cluster of homogeneously distributed charge. The modification due to a Gaussian laser profile is shown in Fig. 1(b). The influence of a size distribution of the cluster target is shown in Fig. 1(c), while Fig. 1(d) shows the combined effect, and finally, in Fig. 1(e), saturation of ionization has been included in addition. We will now discuss the impact of each of these conditions in detail.

The basic mechanism underlying the KEDI in clusters is their Coulomb explosion. It converts the potential energy $E_{\text{coul}}(r)$ of a (partially) ionized cluster atom at a distance r from the cluster center into kinetic energy E . We assume a homogeneous atomic density in the cluster with radius R and N atoms. The probability dP/dr to find an atom at a distance r from the cluster center is then given by

$$\frac{dP}{dr} = \frac{3r^2}{R^3} \Theta(R-r), \quad (1)$$

where $\Theta(x)$ is the step function, which is 1 for $x \geq 0$ and 0 otherwise. If the cluster is charged homogeneously by the laser pulse with charge q per ion and the ions have not moved yet, then the potential (Coulomb) energy of an ion at radius $r \leq R$ inside the cluster is given by

$$E_{\text{coul}}(r, q, N) = Nq^2 r^2 / R^3. \quad (2)$$

The ions at the cluster edge R have the maximum energy, which sets the energy scale $E_R := E_{\text{coul}}(R, q, N) = q^2 N / R$. Since in Coulomb explosion the entire potential energy E_{coul} is converted into kinetic energy E , the combination of Eqs. (1) and (2) gives directly the KEDI [13,15]. Using the characteristic energy scale E_R and defining $\varepsilon = E/E_R$, it reads

$$\frac{dP}{d\varepsilon} = \frac{3}{2} \sqrt{\varepsilon} \Theta(1-\varepsilon). \quad (3)$$

This is the single-cluster KEDI spectrum shown in Fig. 1(a). Note that to obtain this spectrum it is not necessary to follow the trajectories of the particles due to a repulsive Coulomb force as a function of time t , which are known analytically [16,17]. Actually, their asymptotic values ($t \rightarrow \infty$) are sufficient. Consequently, a smooth charging, instead of a sudden one, would change the absolute scale of the KEDI but not its shape. Moreover, the present Coulomb explosion model excludes that ions overtake each other as happens in shock-wave formation [16–18], predicted for other initial densities than the steplike one of Eq. (1). However, it is an open question to what extent such shockwaves persist, if ion-ion correlation is taken into account [19]. Finally, we note that non-homogeneous charge distributions, i.e., $q \rightarrow q(r)$, produce different single-cluster KEDIs. These differences, however, are almost completely masked by the effect of the laser beam

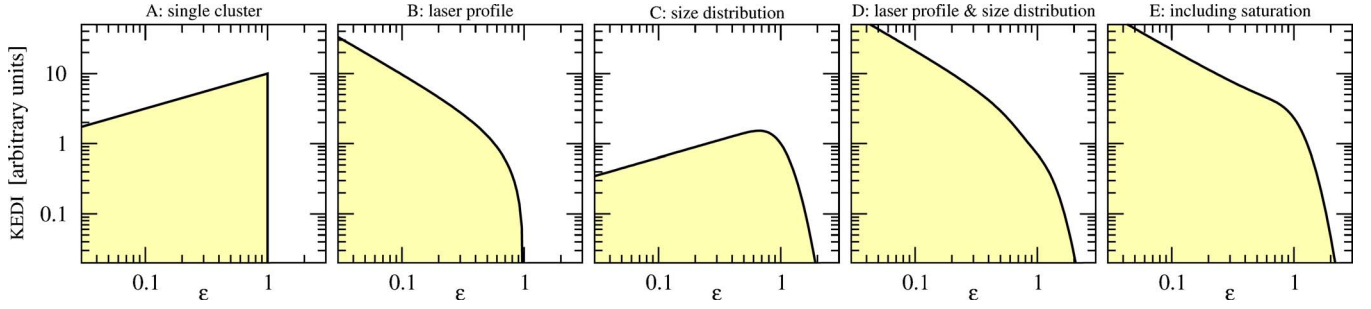


FIG. 1. (Color online) Kinetic-energy distributions of ions (KEDI) for Coulomb exploding clusters as function of a scaled energy ε . See text for the respective definitions. (a) single clusters, cf. Eq. (3); (b) considering a Gaussian laser profile, cf. Eq. (4); (c) assuming a log-normal cluster size distribution, cf. Eq. (6); (d) combining laser profile and cluster size distribution, cf. Eq. (7); (e) including saturation of ionization, cf. Eq. (9).

and the cluster size distribution, as discussed below.

The spatial profile of the laser pulse can usually be described by a Gaussian function so that the field amplitude F is given by $F(\rho) = F_0 \exp(-\rho^2/2\xi^2)$, where F_0 is the field strength at the focus and ρ is the distance (radius) from the laser beam center in the plane perpendicular to the beam. Along the laser beam we assume a constant intensity since the experiments discussed later [12] are performed with a narrow cluster beam, i.e., a radius smaller than the Rayleigh length [20] of the laser beam. This does not hold for the experiments where the cluster beam is irradiated near the output of the gas-jet nozzle [14].

The charging of the cluster is assumed to be proportional to the field strength, $q \propto F$. This applies for resonant charging of the cluster [5,7], where the energy pumped into the cluster is $\propto F^2$ and the Coulomb energy of this cluster $\propto q^2$. As a consequence, we obtain the spatial distribution of charge $q(\rho)$ by replacing $F(\rho)$ with $q(\rho)$ and F_0 with q_0 , where q_0 is the maximum charge per ion obtained in the laser focus at $\rho=0$. Now, one can integrate out the spatial coordinate ρ to obtain the laser profile averaged KEDI, which reads in terms of the scaled energy $\varepsilon = E/E_{\text{coul}}(R, q_0, N)$,

$$\frac{dP_{\text{las}}}{d\varepsilon} = \frac{\pi \xi^2 N}{2} \frac{1 - \varepsilon^{3/2}}{\varepsilon} \Theta(1 - \varepsilon). \quad (4)$$

Its shape is shown in Fig. 1(b). What has changed compared to the original KEDI from Eq. (3) is the qualitatively different behavior with ε^{-1} instead of $\varepsilon^{1/2}$ for small ε . That Eq. (4) formally diverges for $\varepsilon \rightarrow 0$ is an artifact due to neglecting the fact that beyond a maximum radius ρ_{max} the laser intensity is too weak to ionize. This effect can be included at the expense of a more complicated expression. For us, Eq. (4) will suffice. The enhancement of small kinetic energies after averaging over the laser profile is easily understandable from the higher weight of laser intensities less than the peak intensity, which leads to less charging and, consequently, to more ions with smaller kinetic energy.

As it is well known, it is very difficult to produce a beam of mass selected (i.e., size selected) clusters with high enough intensity for laser or other crossed beam experiments. Consequently, the laser beam interacts with clusters of different size N , which are log-normally distributed [21,22] according to

$$g(N) = \frac{1}{\sqrt{2\pi\nu N}} \exp\left(-\frac{\ln^2(N/N_0)}{2\nu^2}\right). \quad (5)$$

Convoluting the single-cluster KEDI from Eq. (3) with $g(N)$ yields in scaled units $\varepsilon = E/E_{\text{coul}}(R, q, N_0)$,

$$\frac{dP_{\text{size}}}{d\varepsilon} = \frac{3}{4} N_0 \sqrt{\varepsilon} \operatorname{erfc}\left(\frac{3 \ln \varepsilon}{2\sqrt{2\nu}}\right). \quad (6)$$

This size-averaged KEDI is shown in Fig. 1(c), the larger the width parameter ν of the cluster size distribution (5) the more its tail reaches beyond the energy $\varepsilon=1$. The fastest fragments are those from the large clusters in the long tail of this distribution. Note that we have assumed the average charge q per fragment to be independent of the cluster size N . We will comment on this assumption below.

Of course, for a realistic experimental KEDI one has to take into account both the spatial profile of the laser beam and the cluster size distribution. This yields, in a similar manner as for the other distributions,

$$\begin{aligned} \frac{dP_{\text{both}}}{d\varepsilon} = & \frac{\xi^2 \pi N_0}{4 \varepsilon} \left[\exp(\nu^2/2) \left(1 + \operatorname{erf}\left(\frac{2\nu^2 - 3 \ln \varepsilon}{2\sqrt{2\nu}}\right) \right) \right. \\ & \left. - \varepsilon^{3/2} \operatorname{erfc}\left(\frac{3 \ln \varepsilon}{2\sqrt{2\nu}}\right) \right]. \quad (7) \end{aligned}$$

Here, we have used $\varepsilon = E/E_0$, with the reference energy $E_0 = E_{\text{coul}}(R, q_0, N_0)$ defined as the maximum Coulomb energy of ions from clusters with the median size N_0 [24] at the laser focus (charge q_0). The corresponding distribution is shown in Fig. 1(d). Since the spatial laser profile modifies the low-energy part and the cluster size distribution the high-energy part of the ion distribution, it is possible to gain information from a measured KEDI on both effects separately.

The final phenomenon that must be taken into account to understand an experimental KEDI is saturation, i.e., the fact that independent of the laser intensity provided, the charging cannot be higher than a certain maximum value q_{sat} , either because the next atomic shell has a much higher ionization potential or because the atoms are completely ionized. We can model the situation by changing our spatial charging function $q(\rho)$ to

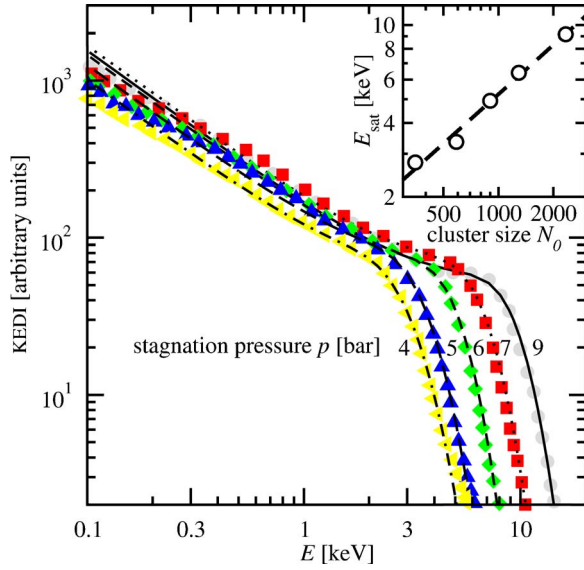


FIG. 2. (Color online) Ion energy spectra according to Eq. (9), shown by lines, fitted to experimental data [12], shown by color/gray symbols. Different stagnation pressures p correspond to different cluster sizes N_0 , cf. the values listed in Table I. Inset: Saturation energy E_{sat} as a function of the cluster size N_0 . The values from Table I (circles) are shown along with the least-square fit of $E_{\text{sat}} = N_0^{0.667} 0.052$ keV (dashed line), with the exponent being in nice agreement with Eq. (10) for a fixed saturation charge.

$$q(\rho) = \begin{cases} q_{\text{sat}} & \text{for } \rho \leq \rho_{\text{sat}}, \\ q_0 \exp(-\rho^2/2\xi^2) & \text{for } \rho > \rho_{\text{sat}}, \end{cases} \quad (8)$$

with q_{sat} the maximum charge, which is realized for clusters close to the center of the laser focus with $\rho < \rho_{\text{sat}}$. The saturation can be characterized by the dimensionless quantity $\eta := q_{\text{sat}}/q_0 \in [0, 1]$. The radius of saturation in Eq. (8) is given by $\rho_{\text{sat}} = \xi \sqrt{-2 \ln \eta}$. The charging function Eq. (8) amounts to using the averaging over the spatial profile only for $\rho > \rho_{\text{sat}}$ and suggests to define the energy scale as $\varepsilon = E/E_{\text{sat}}$ with the saturation energy $E_{\text{sat}} = E_{\text{coul}}(R, q_{\text{sat}}, N_0)$. The result is the KEDI,

$$\frac{dP_{\text{sat}}(\eta)}{d\varepsilon} = \frac{dP_{\text{both}}}{d\varepsilon} - \ln \eta \frac{dP_{\text{size}}}{d\varepsilon}, \quad (9)$$

which develops a characteristic hump before $\varepsilon = 1$, as can be seen in Fig. 1(e).

After having derived the analytical expression for the KEDI, we will now quantitatively compare its shape, as given by Eq. (9), with available experimental data. We begin with experiments [12] on molecular clusters $(N_2)_N$ with $N \approx 300, \dots, 3000$, since this data set provides a systematic study for changing the stagnation pressure p , i.e., different (median) cluster sizes N_0 . Figure 2 shows the measured KEDI [12] along with predictions from our simple model. We have fitted the KEDI from Eq. (9) to each of the experimental data sets and observe an excellent agreement. The model not only predicts the correct asymptotic behavior for small as well as larger energies, but nicely reproduces also the increasingly pronounced humps around the “knees.” The

TABLE I. Parameters of the fitted curves shown in Fig. 2 for different stagnation pressures p , i.e., different cluster sizes N_0 .

p (bar)	size N_0	ν	η	E_{sat} (keV)
4	350	0.44	0.51	2.76
5	590	0.40	0.48	3.34
6	900	0.38	0.46	4.91
7	1295	0.37	0.38	6.40
9	2336	0.36	0.31	9.15

fits were obtained by taking the median cluster size from Hagen’s scaling law [23] for each stagnation pressure p indicated in Fig. 2 (cf. Table I for absolute values of N_0). The obtained fitting parameters ν , η , and E_{sat} are summarized in Table I.

Our model allows one to extract from the measured KEDI directly the width of the cluster size distribution ν , a quantity which is often not known in the experiment. We obtain values of $\nu \approx 0.4$ and observe a decrease for larger clusters. Earlier measurements [21] of the size distribution for larger N_2 clusters yielded log-normal distributions with $\nu = 0.48$.

The very good agreement of model and experiment supports our assumption of a saturation charge, which for the case of nitrogen should be $q_{\text{sat}} = 5$, the number of valence electrons. A common saturation charge would result in a characteristic dependence of the saturation energy E_{sat} on the particle number N . According to Eq. (2) this relation reads

$$E_{\text{sat}} \propto N_0/R \propto N_0^{2/3}. \quad (10)$$

Indeed, this dependence holds as shown by the inset of Fig. 2, which provides further, independent evidence for the saturation phenomenon and our modeling of it.

Finally, we present in Fig. 3 fits to other experimental data. Despite the different cluster targets and laser param-

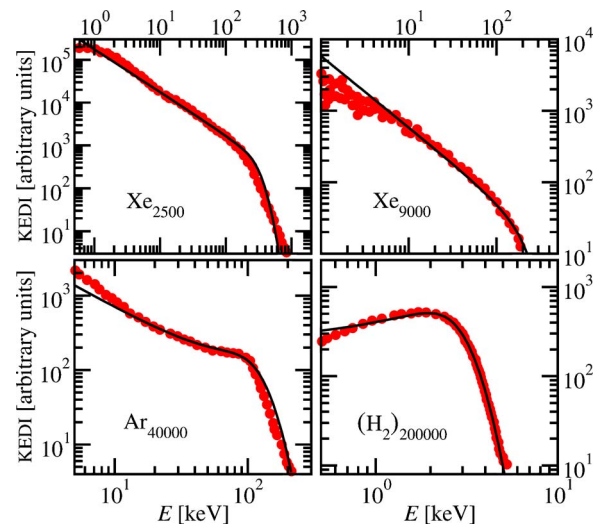


FIG. 3. (Color online) Ion energy spectra for Xe_{2500} [8], Xe_{9000} [9], Ar_{40000} [10], and $(\text{H}_2)_{200000}$ [13] clusters from experiments (circles) and fits by our model (solid line).

eters used in these measurements, our model allows for proper fits of all of them. Whereas xenon clusters do not show any noticeable saturation effect ($\eta=0.8$, upper two graphs in Fig. 3), the large gap between the first and the second shell of argon, similar to the N_2 case, is responsible for the hump seen in the KEDI ($\eta=0.35$, lower left graph in Fig. 3). Hydrogen clusters are extreme cases, since only one electron per atom is available ($\eta=0$, lower right graph in Fig. 3).

We may go one step further and try to obtain dynamical information on the charging process. A comparison of the absolute values of E_{sat} gives information about the radius at which the charging of the cluster occurs, since ionization at a larger radius R results in smaller kinetic energies E . Assuming a smooth charging according to $q(t)=q(t\rightarrow+\infty)/(1+\exp(-t/\Delta T))$, which was observed in microscopic calculations [5], we obtain charging times of $\Delta T\approx 50, \dots, 75$ fs, which should be compared to the experimental pulse length of 100 fs [12]. The corresponding radii are $R(t=0)\approx 3R(t\rightarrow-\infty)$, indicating a fast explosion of the relatively light-weight nitrogen cluster ions.

The smaller saturation parameters η for the larger clusters (cf. Table I) imply a stronger decrease of the average charge

for clusters outside the laser focus, i.e., for $\rho>\rho_{\text{sat}}$. This weaker charging can be understood in terms of a field ionization model [7]. It applies for pulses which are too weak (or too short) to drive a cluster expansion during the pulse in order to reach resonant absorption. In such cases the average charge per ion scales as $q\propto R^{-1}\propto N^{-1/3}$ [7], explaining the decrease for larger clusters.

In summary, we have formulated a simple analytical model for the ion kinetic-energy spectra of laser irradiated clusters. This model allows one to link quantitatively experimental spectra to typical theoretical single-cluster results. We have been able to fit all experimentally available size-dependent KEDIs [8–13], which correspond to the experimental setup in terms of laser profile and cluster distribution we have assumed. As demonstrated, our model is accurate enough to extract even dynamical information on the charging process of the cluster from the spectra. We hope that this link will allow the comparison of observables from cluster experiments with theory on a similar quantitative basis as it is done routinely for atomic or molecular observables.

It is a pleasure to acknowledge very instructive discussions with M. Krishnamurthy.

-
- [1] *Molecules and clusters in intense laser fields*, edited by J. Posthumus (Cambridge University Press, 2001).
 - [2] V. P. Krainov and M. B. Smirnov, *Phys. Rep.* **370**, 237 (2002).
 - [3] T. Ditmire *et al.*, *Phys. Rev. A* **53**, 3379 (1996).
 - [4] H. M. Milchberg, S. J. McNaught, and E. Parra, *Phys. Rev. E* **64**, 056402 (2001).
 - [5] U. Saalman and J. M. Rost, *Phys. Rev. Lett.* **91**, 223401 (2003).
 - [6] C. Jungreuthmayer, M. Geissler, J. Zanghellini, and T. Brabec, *Phys. Rev. Lett.* **92**, 133401 (2004).
 - [7] U. Saalman, *J. Mod. Opt.* **53**, 173 (2006).
 - [8] T. Ditmire *et al.*, *Nature (London)* **386**, 54 (1997).
 - [9] E. Springate *et al.*, *Phys. Rev. A* **61**, 063201 (2000).
 - [10] V. Kumarappan, M. Krishnamurthy, and D. Mathur, *Phys. Rev. Lett.* **87**, 085005 (2001).
 - [11] V. Kumarappan, M. Krishnamurthy, and D. Mathur, *Phys. Rev. A* **67**, 043204 (2003).
 - [12] M. Krishnamurthy, D. Mathur, and V. Kumarappan, *Phys. Rev. A* **69**, 033202 (2004).
 - [13] S. Sakabe *et al.*, *Phys. Rev. A* **69**, 023203 (2004).
 - [14] M. Hirokane *et al.*, *Phys. Rev. A* **69**, 063201 (2004).
 - [15] J. Zweiback *et al.*, *Phys. Plasmas* **9**, 3108 (2002).
 - [16] A. E. Kaplan, B. Y. Dubetsky, and P. L. Shkolnikov, *Phys. Rev. Lett.* **91**, 143401 (2003).
 - [17] V. Yu. Bychenkov and V. F. Kovalev, *Plasma Phys. Rep.* **31**, 178 (2005).
 - [18] F. Peano, R. A. Fonseca, and L. O. Silva, *Phys. Rev. Lett.* **94**, 033401 (2005).
 - [19] T. Pohl, T. Pattard, and J. M. Rost, *Phys. Rev. A* **70**, 033416 (2004).
 - [20] A. E. Siegman, *Lasers* (University Science Books, Sausalito, 1986), Chap. 17.
 - [21] J. Gspann, in *Physics of Electronic and Atomic Collisions*, edited by S. Datz (North-Holland, Amsterdam, 1982), p. 79–92.
 - [22] M. Lewerenz, B. Schilling, and J. P. Toennies, *Chem. Phys. Lett.* **206**, 381 (1993).
 - [23] O. F. Hagen and W. Obert, *J. Chem. Phys.* **56**, 1793 (1972).
 - [24] The median size N_0 separates the higher half of the distribution from the lower half. In a log-normal distribution it is different from the average size, which is $\exp(\nu^2/2)N_0$.